Biochemistry and Biophysics Reports 3 (2015) 108–116

Contents lists available at ScienceDirect

Biochemistry and Biophysics Reports

journal homepage: www.elsevier.com/locate/bbrep

The stability of the TIM-barrel domain of a psychrophilic chitinase

Philemon Stavros [a,b], Piotr H. Malecki [c], Maria Theodoridou [a], Wojciech Rypniewski [c], Constantinos E. Vorgias [d], George Nounesis [a,*]

[a] Biomolecular Physics Laboratory, INRASTES, National Centre for Scientific Research "Demokritos", 153 10 Aghia Paraskevi, Greece
[b] Physics Department, National and Kapodistrian University of Athens, 157 01 Zografou, Greece
[c] Institute of Bioorganic Chemistry, Polish Academy of Sciences, Noskowskiego 12/14, 61-704 Poznan, Poland
[d] Department of Biochemistry and Molecular Biology, National and Kapodistrian University of Athens, 157 01 Zografou, Greece

ARTICLE INFO

Article history:
Received 19 June 2015
Received in revised form
24 July 2015
Accepted 28 July 2015
Available online 30 July 2015

Keywords:
Stability
Thermodynamics
Unfolding
Psychrophilic TIM-barrel
Chemical denaturation
Calorimetry

ABSTRACT

Chitinase 60 from the psychrophilic bacterium Moritella marina (MmChi60) is a four-domain protein whose structure revealed flexible hinge regions between the domains, yielding conformations in solution that range from fully extended to compact. The catalytic domain is a shallow-grooved TIM-barrel. Heat-induced denaturation experiments of the wild-type and mutants resulting from the deletions of the two-Ig-like domains and the chitin binding domain reveal calorimetric profiles that are consistent with non-collaborative thermal unfolding of the individual domains, a property that must be associated to the "hinge-regions". The calorimetric measurements of the $(\beta/\alpha)_8$ catalytic domain reveal that the thermal unfolding is a slow-relaxation transition exhibiting a stable, partially structured intermediate state. Circular dichroism provides evidence that the intermediate exhibits features of a molten globule i.e., loss of tertiary structure while maintaining the secondary structural elements of the native. GdnHCl-induced denaturation studies of the TIM-barrel demonstrate an extraordinarily high resistance to the denaturant. Slow-relaxation kinetics characterize the unfolding with equilibration times exceeding six days, a property that is for the first time observed for a psychrophilic TIM barrel. On the other hand, the thermodynamic stability is $\Delta G = 6.75 \pm 1.3$ kcal/mol, considerably lower than for structural-insertions-containing barrels. The mutant E153Q used for the crystallographic studies of MmChi60 complexes with NAG ligands has a much lower stability than the wild-type.

1. Introduction

Chitinases (EC 3.2.1.14) hydrolyse chitin, the linear, insoluble β-1,4-linked polymer of *N*-acetyl-*β*-D-glucosamine, which is abundant in nature since it is an important element in the structure of fungal cell walls, shells, arthropod, worm and molluscs exoskeletons, including crustaceans and insects [1]. Chitin, with approximately 10^{11} t produced annually in the aquatic biosphere [2], is considered to be a valuable raw material for a multitude of agricultural and biomedical applications [3]. Since the major part of the marine biosphere is an environment of permanently low temperatures, enzymes from cold-adapted psychrophilic bacteria and microorganisms present particularly interesting systems and mechanisms to explore. Chitinases produced by psychrophilic bacteria have high catalytic activities at low-temperature conditions while exhibiting high thermosensitivity, properties that render them excellent candidates for many applications [4]. Until recently though only a handful of psychrophilic chitinases have been isolated from bacteria [5–7] etc.

Based on primary structure comparisons, chitinases have been classified in families 18 and 19 of the glycosyl hydrolase superfamily [8]. Several common properties are shared by the members of a family such as the folding of the catalytic domain, the substrate specificity, the stereochemistry of the reaction as well as the catalytic mechanism [9] and [10]. Differences in amino-acid sequences and 3D structures [11] though between the two families indicate evolution from different ancestors [12].

In general, bacterial chitinases are characterized by a multi-domain architecture [13]. Their common feature is a catalytic domain with a (β/α), TIM-barrel fold. Many catalytic domains contain an additional α+β insertion domain or extended loops inserted in the TIM-barrel, which participate in the structure of the substrate binding groove by essentially making it deeper or even tunnel-like. Chitinases often exhibit carbohydrate binding modules, which are designed to bind chitin (carbohydrate-binding module-CBM) [14].

* Corresponding author.
E-mail address: nounesis@rrp.demokritos.gr (G. Nounesis).

http://dx.doi.org/10.1016/j.bbrep.2015.07.016

In addition, fibronectin type III (Fn3) or immunoglobin-like (Ig-like) domains [15,16] can also be encountered, which are believed to play the role of spacers, able to adjust the position of the CBM relative to the catalytic domain.

The TIM-barrel fold which is among the most ancient, frequent and versatile [17,18] has attracted considerable experimental and theoretical interest [19]. Chemical unfolding/refolding studies along with molecular simulations and modeling have consistently revealed slow-relaxation kinetics and demonstrated the presence of thermodynamically stable intermediate states possessing various degrees of structure compared to the native fold. Thus, a 6+2 mechanism has been proposed for the folding of the β/α-barrel [20] although a 4+2+2 mechanism has also been shown to be feasible [21] by simulation studies. The recent study of an extremely thermostable β/α-barrel revealed a two state-unfolding characterized by a high kinetic barrier protecting the molecule from chemical denaturation. The unfolding kinetics were found to be extraordinarily slow, taking over six weeks to attain equilibrium at room temperature [22]. Few experiments have been carried out to measure the thermodynamic stability based on the heat-induced denaturation of TIM-barrels. Chitinase 40 from the thermophilic *Streptomyces thermoviolaceus* exhibited reversible non-two-state thermal unfolding, displaying once more slow relaxation kinetics [23]. The non-two state character was proposed to be directly associated to the α+β insertion of the β/α-barrel. Analogously, calorimetric results for the mesophilic chitinase-A from *Serratia marcescens* demonstrated the important contribution of the α+β insertion to the overall stability of the protein [24].

Recently the complex structure of a multidomain psychrophilic chitinase 60 from the bacterium *Moritella marina* (*Mm*Chi60) has been solved [15] in an unliganded form and for the E153Q mutant in a complex form with NAG_4 and NAG_5 [25]. The cold-adapted bacterium produces chitinase to utilize chitin as a source of carbon, nitrogen and energy [26]. The structure consists of four domains: The catalytic TIM-barrel, bare of any loop or other domain insertions and thus characterized by only a shallow groove at the active center, two Ig-like domains and a chitin-binding domain (ChB). Hinge regions connect the domains providing high-flexibility to the molecule (Fig. 1) [15]. Indeed, SAXS experiments of *Mm*Chi60 in solution revealed that it can exist in different conformations ranging from fully extended to compact [25].

In this paper we present our work on the thermodynamic stability of *Mm*Chi60 in solution, the first of its kind for a psychrophilic chitinase. We demonstrate the effects of the hinge regions upon the calorimetric profile of the molecule. We systematically focus the study on to the unfolding properties of the TIM-barrel by carrying out heat-induced- and chemical denaturation experiments on mutants bearing deletions of the Ig-like and the ChB domains. We show the impact on the protein stability of the point E153Q mutation, widely used for the liganded crystallographic studies. For our studies we employed a variety of biophysical techniques including high-accuracy adiabatic DSC, circular dichroism and fluorescent spectroscopy.

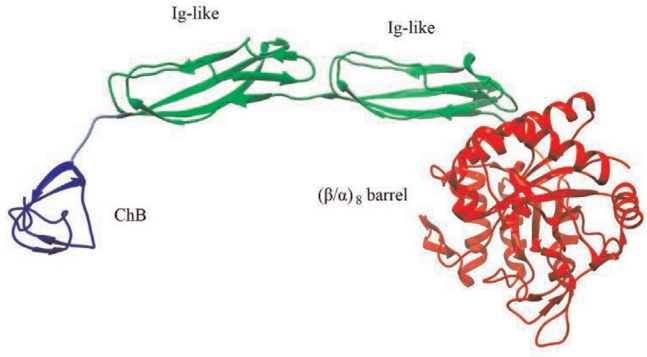

Fig. 1. Ribbon representation of the *Mm*Chi60 structure illustrating the four domains of the protein (Ref. [15], PDB entry 4hmc).

2. Experimental methods

2.1. Plasmid and DNA manipulations

The chitinase gene named *Mm*Chi60 from *Moritella marina* was cloned as described in [26]. T7 expression vectors, pET-11a bearing the *Mm*Chi60 gene, were isolated using Plasmid Miniprep DNA Purification Kit (EURx, Poland) and mutations were introduced into plasmids. The active-site mutant was prepared by introducing an E153Q mutation by site-directed mutagenesis as described in [15]. *Mm*Chi60 deletion mutants *Mm*Chi60Cat-(ΔT346-R550) and *Mm*Chi60Δ(Ig1)Δ(Ig2)-(ΔM348-A504) were prepared using the PIPE method which takes advantage of the observation that, contrary to the common assumption, normal PCR amplification results is a mixture of products, which are not fully double stranded. The 5′ ends of the reaction product (which are exactly the same fragments as delivered by the synthetic primers) can be left unpaired in the final round of PCR. Therefore, simply by changing the primer sequence of those ends, mutation can be promoted in a simple PCR reaction without additional steps [27]. Both primers were designed to flank the deletion part of the enzyme to amplify the plasmid except for the part to be deleted. The PCR reactions were performed using the primers: *Mm*Chi60Cat: forward primer: CAATTACCCCCAGTGTAAGGATCCGGCTGCTAACAAAGCC, reverse primer: CAGCCGGATCCTTACACTGGGGGTAATTGATTATGAATAAAGTTACC *Mm*Chi60Δ(Ig1)Δ(Ig2) forward primer: CCAGTGACAGATGTAAGTGATGATGATTGG CAAGTAGGCAG, reverse primer: CAATCATCATCACTTACATCTGTCACTGGGGGTAA TTGATTATGAATAAAG. The underlined fragment of the primers is complementary to the second primer's binding fragment.

2.2. Overproduction and purification of the mutated enzyme

All mutants were overproduced and purified as it is described in [15] for *Mm*Chi60_E153Q mutant. Briefly, the cell culture was grown in Luria Bertani (LB) medium containing 100 μg/ml ampicillin and 50 μg/ml kanamycin at 37 °C. Enzyme expression was induced with 1 mM isopropyl-D-1-thiogalactopyranoside (IPTG) at the mid-exponential growth phase and the culture was further incubated at 18 °C overnight. Advantage was taken of the fact that the protein of interest is localized in the periplasm. Cells were broken by osmotic shock according to a previously published procedure with some alternations [28]. *E. coli* cells were suspended and mixed for 10 min in osmotic buffer consisting of 20% (w/v) sucrose, 0.03 M Tris–HCl, 3 mM EDTA and centrifuged at 6000 r.p.m. in a JLA 10.500 rotor (Beckman). The cells were resuspended in ice-cold water and the periplasmic proteins were released into the solution by mixing the cold solution for 10 min. The cells were centrifuged at 10000 rpm in a JLA 10.500 rotor (Beckman) and the clear supernatant was adjusted to 1 M ammonium sulfate, 20 mM sodium phosphate buffer pH 8.0 and directly applied onto a 10 ml Phenyl-Sepharose 6 Fast Flow column, previously equilibrated in the same buffer (GE Healthcare). The column was washed with the same buffer and the bound proteins were eluted by descending linear gradient of ammonium sulfate from 1 M to 0 M. Fractions containing the *Mm*Chi60 mutant were combined, concentrated and applied onto a Superde × 200 gel-filtration column (1.6 60 cm, Pharmacia) in 20 mM Tris buffer, 200 mM NaCl pH 8.0. The enzymes purity was assessed by 0.1% SDS, 12.5% PAGE according to Laemmli, 1970 followed by Coomassie Brilliant Blue staining. The concentration of the various

forms of chitinase was determined from the absorption at 280 nm using an UV spectrophotometer. The extinction coefficient of the protein was estimated on the basis of the amino acid sequence using the Expasy's ProtParam tool [29].

2.3. High-accuracy adiabatic-DSC

The VP-DSC differential scanning calorimeter (MicroCal Inc., Northampton, MA, USA) was employed to explore the thermal unfolding of *Mm*Chi60 and its mutants. High-accuracy measurements of the heat capacity at constant pressure ($\langle\Delta C_p\rangle$) vs. temperature (T) are collected as T is raised continuously from room temperature to above the denaturation temperature. Protein concentrations were used in the range of 0.5–1.4 mg/mL. Seven reference scans with only buffer-filled cells (volume of 0.523 mL) preceded each data-acquisition run in order to eliminate device thermal history effects and achieve maximum baseline repeatability. Protein and buffer solutions were thoroughly degassed under vacuum prior to loading to the calorimeter. The heating scanning rate (u) was selected between 0.17 and 1.5 K/min. The reversibility of the calorimetric data was tested by performing a second consecutive heating scan and comparing the results for the total enthalpy (ΔH). Whenever needed, the difference in the heat capacity between the initial and the final state was modeled by a sigmoidal chemical baseline [30]. The calorimetric data have been analyzed via nonlinear least square fitting procedures of ORIGIN 9.0 software.

2.4. Circular dichroism

Circular dichroism (CD) spectra have been collected with a JASCO J-715 spectropolarimeter (JASCO, Easton, MD), equipped with a JASCO PTC 348 WI temperature controller, in the 190–360 nm wavelength range, using properly sealed quartz cuvettes. In the far-UV region (190–260 nm), protein samples with concentrations 0.14 and 0.1 mg/mL for the wild-type and the mutant were loaded into a 0.1 cm path-length quartz cuvette (HELMA), while in the near-UV region (260–360 nm), protein samples with concentrations 0.6 and 0.3 mg/mL for the wild-type and the mutant were loaded into a 1 cm path-length cuvette. Five to seven spectra were accumulated and averaged for each experiment, with a wavelength step 0.2 nm at a rate 50 nm min^{-1}, a response time of 2 s and a bandwidth of 1 or 2 nm. Buffer spectra, obtained at identical conditions, have been subtracted from the sample ones.

2.5. Chemical denaturation

Chemical denaturation experiments have been carried out using a QuantaMaster UV VIS spectrofluorometer (Photon Technology International, Inc. Birmingham, UK) using Guanidine-Hydrochloride (GndHCl) as denaturant. The experiments were carried out at 20 °C. Protein solutions of 0.04–0.08 mg/mL were added in a 4 mL quartz fluorometer cuvette and the intrinsic protein fluorescence was measured using the following parameters: excitation wavelength 295 nm, excitation slit width 0.55 nm, emission slit width 0.7 nm, integration time 20 s. The fluorescence spectra were collected in the range from 300 to 450 nm. Significant changes were continuously observed in the emission spectra of protein samples, in the presence of various amounts of GndHCl, for unusually long times. In order to design accurate experiments, protein solutions containing chemical denaturant concentrations from 0.5 to 3 M were prepared simultaneously and were consequently stored in Eppendorf tubes in the dark for several days, in order to achieve chemical equilibrium. The background signal (fluorescent or scattered light) from the buffer was measured separately and was subsequently subtracted from the raw data.

3. Results and discussion

The heat-induced unfolding of *Mm*Chi60 was studied by high-accuracy DSC. A heating scan rate of 1.5 K/min was applied. Reversible calorimetric profiles i.e. excess heat capacity ($\langle\Delta C_p\rangle$) vs. temperature (T) plots, have been obtained at pH 8.0, 20 mM sodium phosphate 1 mM EDTA buffer, displaying three distinct thermal anomalies: a prominent peak at $T_1=55.8$ °C and two weak features at $T_2=44.7$ and $T_3=35.1$ °C, as shown in Fig. 2 (bottom panel). The reversibility expressed as the ratio of the total enthalpy change between two consecutive heating scans was higher than 90% for the main peak and ~80% for the two smaller ones. The consistency between the calorimetric profiles at various concentrations of *Mm*Chi60, confirms the monomeric state of the molecule in the chosen buffer. The complex DSC profile can be directly associated to the structural characteristics of the *Mm*Chi60 molecule, displaying enhanced flexibility, arising from the very unique architecture of the hinge regions between the various domains of the protein. An uncooperative unfolding of the four domains may thus be anticipated resulting into the observed trio

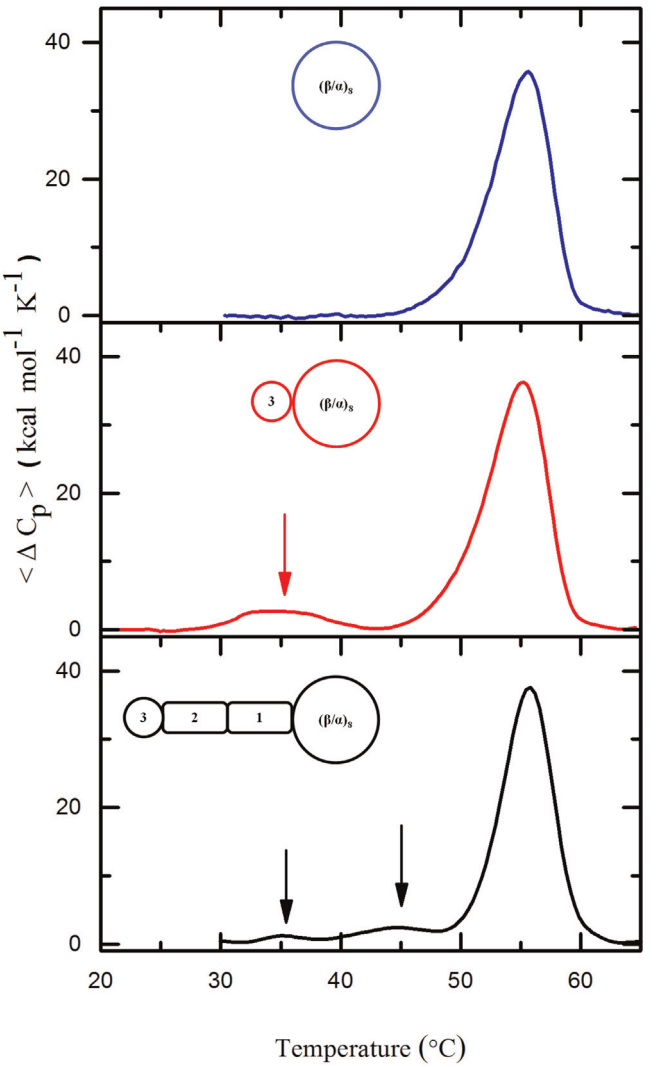

Fig. 2. DSC profiles of heating scans of *Mm*Chi60 (bottom panel) in pH 8.0, 20 mM sodium phosphate 1 mM EDTA buffer as well as of two mutants bearing the deletion of the two Ig-like domains *Mm*Chi60Δ(Ig1)Δ(Ig2) (middle panel) as well as *Mm*Chi60Cat, bearing the deletion of the Ig-like and the ChB domains, i.e. with only the TIM barrel catalytic domain remaining (top panel). For all the scans the heating rate $u=1.5$ K/min. The arrows indicate the heat capacity anomalies associated with the thermal unfolding of the two Ig-like domains and the ChB domain.

of thermal anomalies (where the two Ig-like domains are expected to unfold cooperatively). In addition, the two low-temperature peaks may also include enthalpic contributions arising from temperature-dependent transformations between the different molecular conformations, from compact to fully extended, as these were revealed by recent SAXS experiments [25]. By calculating the per-residue enthalpy changes (ΔH) for each of the three peaks the following results are obtained: $\Delta H(T_1)$ 0.65 ± 0.04 kcal/mol-residue, $\Delta H(T_2)=0.11 \pm 0.01$ kcal/mol-residue, $\Delta H(T_3)=0.28 \pm 0.03$ kcal/mol-residue. The values for the peaks at T_3 and especially at T_2 are considerably lower compared to what is expected for the unfolding of small globular proteins [31]. In this sense, these two minor peaks may be describing only the partial denaturation of domains or even reflecting the fact that the unfolding of the flexible "hinge" regions may only have a small contribution to the measured enthalpy changes. Nevertheless, small enthalpy contributions resulting from heat-induced conformational transitions of the *Mm*Chi60 molecules from the more compact to the fully extended, elongated structure cannot be excluded either.

In order to better understand the DSC results, two mutants of *Mm*Chi60 have been overexpressed and purified, *Mm*Chi60Δ(Ig1)Δ(Ig2) bearing a deletion of the two Ig-like domains, residues 348–504 and *Mm*Chi60Cat where the ChB domain is also removed (ΔT346-R550) and the molecule comprises exclusively of the β/α-barrel structural motif, residues 23–346. Indeed, as it can be seen in Fig. 2, in the reversible DSC calorimetric profile of *Mm*Chi60Δ(Ig1)Δ(Ig2) only two thermal anomalies can be detected. Once again the calorimetric results were found to be independent of protein concentration providing evidence for the monomeric state of the mutant. The main feature at $T_1=55.2$ °C and a second peak at a lower temperature $T=34.9$ °C comparable to T_3 in the *Mm*Chi60 profile. In other words, it appears that following the deletion of the two Ig-like domains, the second lowest in temperature peak T_2 has vanished from the DSC profile. Interestingly, the two remaining peaks are characterized by comparable per-residue enthalpy changes: $\Delta H(T_1)$ 0.73 ± 0.04 kcal/mol-residue, $\Delta H(T_3)=0.97 \pm 0.10$ kcal/mol-residue. Finally, in the case of the *Mm*Chi60Cat mutant, only the main calorimetric peak at $T=55.6$ °C remains as the sole anomaly of the DSC profile, characterized by $\Delta H(T_1)$ 0.70 ± 0.04 kcal/mol-residue, describing thus the heat-induced unfolding of the TIM barrel. All these results provide substantial evidence that thermal unfolding of the domains of *Mm*Chi60 molecule take place independently of each other at a temperature range that is approximately twenty degrees wide. By assigning the T_2-peak to the unfolding of the two Ig-like domains and consequently the T_3 to the unfolding of the ChB it becomes evident that the latter can only function below 36 °C, which may in turn be significant of a very characteristic evolutionary property of the psychrophilic organism *Moritela marina*. It is worth noting at this point that in the case of chitinase-A from *Serratia marcenses* the mutant bearing a deletion of the α+β insertion in the catalytic TIM barrel domain, also displays a heat-induced unfolding, likely associated with the chitin binding domain at ~35 °C [24].

Interestingly, as it can be observed for all three thermograms displayed in Fig. 1, the main heat capacity anomalies display a remarkable consistency in the T_m values and only small differences in ΔH and the full width at half maximum of the peaks, which is often associated with the cooperativity of the thermal transition. A direct comparison of the characteristics of these peaks provides evidence that the thermal unfolding of *Mm*Chi60Cat, i.e. of the TIM-barrel, is characterized by higher per residue enthalpy (0.70 kcal/mol-residue) compared to native *Mm*Chi60 and also lower cooperativity even though the melting temperature T_m remains relatively unaffected (Table 1). These findings are not surprising given the fact that the initial and final states for the unfolding transition of each of the three molecules may indeed be different. We have thus proceeded in a systematic study of the thermodynamic stability of the *Mm*Chi60Cat mutant since it represents the first stable, chitinase TIM-barrel catalytic domain that is free of (α+β)-domain albeit having a small β–hairpin insertion (residues 218–235).

Heat denaturation experiments of the β/α-barrel have been carried out in pH 8.0, 20 mM sodium phosphate 1 mM EDTA buffer at various protein concentrations C_t ranging from 0.5 to 1.0 mg/ml. While the heat capacity anomalies and especially T_m (temperature for maximum ΔC_p value) are independent of C_t, as expected for a monomeric protein, a pronounced dependence on the heating scan rate has been recorded. The ($\langle \Delta C_p \rangle$) vs. ($T$) calorimetric curves at four different DSC heating scan rates (u) and $C_t=0.8$ mg/ml are displayed in Fig. 3. For the four profiles, the population of denatured molecules, refolding to the native state upon very fast cooling, as this can be established by a consecutive second heating run through the denaturation transition, varied as follows: for $u=1.5$ K/min, 92% of the molecules have refolded upon cooling to room temperature, 95% for $u=1.0$ K/min, 89% for $u=0.5$ K/min and 70% for $u=0.33$ K/min. The recorded irreversibility trend appears to be dependent upon the total time the sample remains at high temperatures, in the unfolded state. This directly points to kinetically-driven, slow aggregation processes taking place at the unfolded state, not inherent to the transition itself. On the other hand the strong dependence of the thermal anomalies upon the heating scan rate can be straightforwardly considered a manifestation of the fact that equilibrium relaxation during the thermal unfolding is indeed slower than the applied heating rates.

A kinetic analysis of the calorimetric data has been attempted based upon a two-state reversible model

$$N \underset{k_r}{\overset{k_d}{\leftrightarrows}} D$$

The rate of change of the population of molecules (α) in the denatured state at is given by

$$\frac{da}{dt} = k_d(1 - a) - k_r a \quad (1)$$

The temperature dependence of α is given by

Table 1
Calorimetric parameters describing the peaks in the DSC profiles of *Mm*Chi60 and the two mutants: *Mm*Chi60Δ(Ig1)Δ(Ig2) and *Mm*Chi60Cat. For obtaining the per-mol-residue of the enthalpy of unfolding $\Delta H(T_x)$ the following numbers of residues have been considered: For the TIM-barrel domain at T_1, 319 residues, for the two Ig-like domains at T_2, 151 residues and for the chitin-binding domain at T_3, 24 residues. $\Delta T(T_x)$ is the full width at half maximum of each DSC peak, reflecting the degree of cooperativity in the thermal unfolding of each domain.

	T_1 (°C)	$\Delta H(T_1)$ (kcal/mol-residue)	$\Delta T(T_1)$ (°C)	T_2 (°C)	$\Delta H(T_2)$ (kcal/mol-residue)	$\Delta T(T_2)$ (°C)	T_3 (°C)	$\Delta H(T_3)$ (kcal/mol-residue)	$\Delta T(T_3)$ (°C)
*Mm*Chi60	55.81	0.65 ± 0.04	4.82	44.73	0.11 ± 0.01	7.39	35.12	0.28 ± 0.03	5.91
*Mm*Chi60Δ(Ig1)Δ(Ig2)	55.24	0.73 ± 0.04	5.88	–	–	–	34.86	0.97 ± 0.10	8.29
*Mm*Chi60Cat	55.64	0.70 ± 0.04	5.41	–	–	–	–	–	1

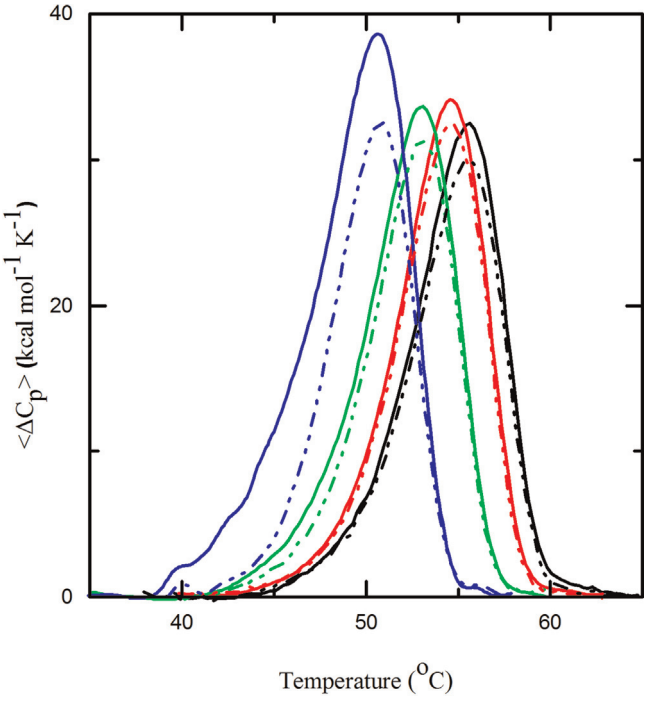

Fig. 3. Reversibility and slow relaxation of the thermal unfolding of the TIM-barrel domain of *Mm*Chi60: First (solid lines) and second consecutive DSC scans (dash-dotted lines) at various heating rates $u=1.5$ K/min (black), 1.0 K/min (red), 0.5 K/min (green) and 0.17 K/min (blue) (For interpretation of the references to color in this figure legend, the reader is referred to the web version of this article.)

$$a(T) = \frac{\Delta h_{\mathrm{cal}} T}{\Delta H_{\mathrm{cal}}} \tag{2}$$

here, ΔH_{cal} is the total calorimetric enthalpy and Δh_{cal} (T) the enthalpy at any temperature T.

By differentiating Eq. (2) with respect to time (t) one gets

$$\frac{da}{dt} = \left(\frac{1}{\Delta H_{\mathrm{cal}}}\right)\left[\frac{d\Delta h_{\mathrm{cal}}(T)}{dT}\right]\left(\frac{dT}{dt}\right) \tag{3}$$

Combining Eqs. (1) and (3) leads to

$$\frac{u\langle \Delta C_p \rangle(T)}{\Delta H_{\mathrm{cal}}} = k_d(T) - \left[k_{\mathrm{d}}(T) + k_{\mathrm{r}}(T)\right]a(T) \tag{4}$$

The results for k_{d} and k_{r} from linear fits of the calorimetric data for the four scan rates u, obtained at six different temperatures $T=49$, 50, 51, 52, 53 and 54 °C, to Eq. (4) are listed in Table 2. The linear fits are presented in Fig. 4. As it can be straightforwardly observed the values for k_{r} are virtually zero at any given temperature. This signifies that denatured protein molecules fail to refold within the available experimental times, or in other words that chemical equilibrium is severely compromised regardless of the high degree of reversibility of the calorimetric data. It is thus

Table 2
Estimates for the denaturation (k_{d}) and refolding (k_{r}) rates as obtained from linear fittings of Eq. (4) for the four different scan rates u, at six different temperatures $T=49$, 50, 51, 52, 53 and 54 °C. The data are displayed in Fig. 3 (lower panel).

T (°C)	K_{d} (h^{-1})	K_{r} (h^{-1})
49	2.14 ± 0.13	~ 0
50	3.17 ± 0.10	~ 0
51	5.15 ± 0.02	~ 0
52	8.04 ± 0.11	~ 0
53	12.43 ± 0.29	~ 0
54	18.85 ± 0.63	~ 0

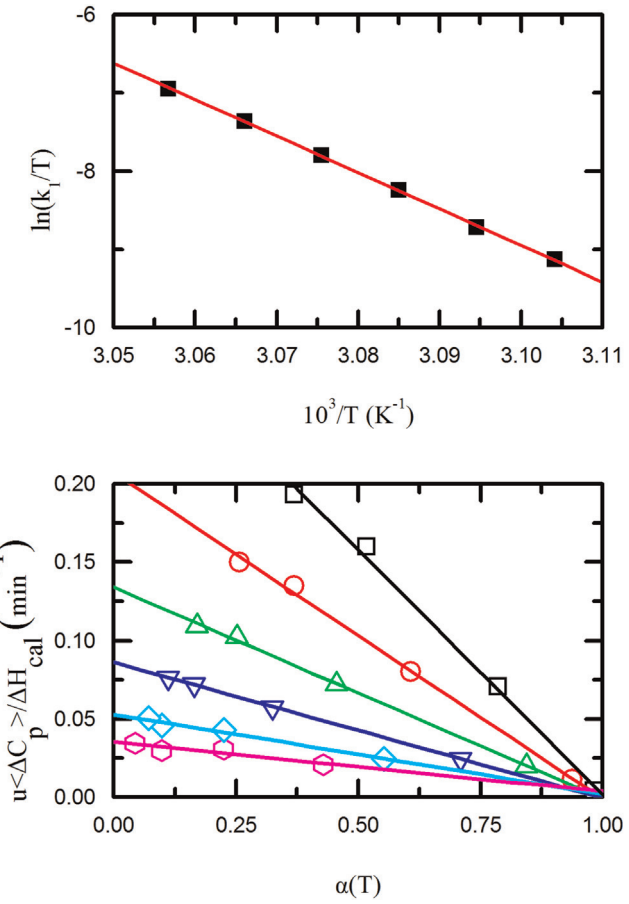

Fig. 4. Slow relaxation kinetics for the thermal unfolding of the $(\beta/\alpha)_8$ barrel of *Mm*Chi60: Lower panel, linear fits of the quantity $[u^*\langle \Delta C_p \rangle/\Delta H_{\mathrm{cal}}]$ vs. the fraction of unfolded molecules (α), providing estimates of the $k_{\mathrm{d}}(T)+k_{\mathrm{r}}(T)$ rates (see Eq. (4) in main text): hexagons correspond to 49, rhombs to 50, down triangles to 51, up triangles to 52, circles to 53 and squares to 54 °C; Upper panel, Eyring plots of the $\ln(k_{\mathrm{d}}(T)/T)$ vs. $1/T$, leading to an estimate of the activation energy $E_{\mathrm{a}}=92.5 \pm 0.7$.

imperative that solely a kinetic analysis based on an irreversible two-state model can be performed. Indeed by fitting the present k_{d} results to an Eyring equation [32], the activation energy $E_{\mathrm{a}}=92.5 \pm 0.7$ kcal/mol can be estimated. This is relatively high compared to other literature reports [33].

The situation of calorimetric but not thermodynamic reversibility is relatively unusual in the literature ([34] and [35]). It has been demonstrated, among others, for the thermal unfolding of the thermophilic PCP-0SH protein where a second-heating DSC peak can only by obtained after allowing the protein solution to remain for 36 h at low-temperatures. A moderate kinetic dependence of the DSC results has also been recorded for the thermal unfolding of the thermophilic Chitinase 40 (Chi40) [23]. In this case though the apparent T_{m}s at various heating rates converge, so that at the lowest, device-dependent heating rate $u=0.17$ kcal/mol, the experimental results coincide with the theoretical projection limit of zero heating rate. In the case of the psychrophilic *Mm*Chi60 such convergence has not been found even though good reversibility is exhibited for the lowest heating rate. This is likely significant of an endogenous characteristic of the specific TIM-barrel.

The heat-induced denaturation of the Chi40 revealed that the calorimetric data could only be fitted using either a non-two-state sequential model involving one equilibrium intermediate or an independent-transitions model involving the unfolding of two energetic domains to intermediate states [23]. In either case, the unfolding of the $\alpha+\beta$ insertion domain has been pointed out as

being possibly related to the non-two-state calorimetric findings. In the case of the present $(\beta/\alpha)_8$ catalytic domain of *Mm*Chi60, any attempt to fit the DSC results, at any heating rate, by a two-state model has produced statistically poor results. Moreover the calorimetric to the van′t Hoff enthalpy ratio was found to vary from 1.5 at the heating rate $u=1.5$ K/min, to 2.0 at the rate of $u=0.33$ K/min. These findings provide evidence for a substantial deviation from two-state models [36]. It is thus becoming apparent that the thermal denaturation of the TIM-barrel of *Mm*Chi60 may also involve an unfolding intermediate. This is a particularly interesting finding since the specific domain, in contrast to Chi40, does not contain the $(\alpha+\beta)$-domain insertion.

CD spectropolarimetry has also been employed in order to investigate the thermal denaturation of the TIM-barrel of *Mm*Chi60 by recording spectroscopic changes at various temperatures through the unfolding transition. In the far-UV, at 25 °C, the spectra for *Mm*Chi60 and *Mm*Chi60Cat analyzed via CDNN reveal differences in the α-helical content but a remarkable convergence as far as the β-sheets. Of course all the CD results can only be compared to the crystallographic findings which only exist for the wild-type *Mm*Chi60. It must thus be deduced that the mutant maintains the structural characteristics of the wild-type barrel, i.e. before the deletion of the other domains takes place. While it is difficult to conceive that the deletion of the side domains can induce structural changes upon the TIM-barrel, changes in the overall geometry of the β-sheets cannot by excluded, leading to a possible widening of the CD zones [37]. The temperature-dependent CD measurements for *Mm*Chi60Cat are displayed in Fig. 5 in the far- (left panel) and near-UV (middle panel). For the far-UV measurements the protein solution was used at a concentration of 0.1 mg/ml while for near-UV at 0.3 mg/ml. Of particular interest are the results presented in the right panel of Fig. 5. They illustrate the temperature dependence of the ellipticity at 200 and 272 nm. A remarkable thermal hysteresis of about three degrees exists for the thermal transition recorded at these two wavelengths. Based on the near-UV data the melting temperature is estimated at 49.9 ± 0.4 °C while from the far-UV measurements the value of 52.9 ± 0.1 °C is obtained. The ellipticity changes at 200 nm are of course associated to changes in the secondary structure of the molecule while at 272 nm with the tertiary structure. It is thus evident that upon heating the TIM-barrel of *Mm*Chi60 from room temperature, the molecule losses first it's tertiary structure and at a three-degree-higher temperature it loses its secondary structure. This result is indicative of a thermodynamically stable intermediate state, in the temperature range of these three degrees, that bears the characteristics of a molten globule state [38,39]. This is the first evidence that a molten globule may be a folding/unfolding intermediate for a TIM-barrel structural motif. Further investigations are required in order to fully confirm it. Interestingly, the Burst-Phase Intermediate state recorded in kinetically controlled refolding experiments of HisF, a *β/α*-barrel protein, is also characterized by substantial secondary and no tertiary, structure based on CD measurements [22].

Since the heat-induced denaturation of the $(\beta/\alpha)_8$ catalytic domain of *Mm*Chi60 was kinetically controlled, thus preventing the measurement of the molecule's thermodynamic stability, GdnHCl-induced chemical denaturation has also been attempted. Chemical denaturants can inhibit the aggregation of denatured molecules establishing thus that chemical denaturation is a thermodynamically controlled process [40]. The bottom panel of Fig. 6 displays raw data, which are fluorescence emission spectra at 300–450 nm, after tryptophan residues have been activated at an excitation wavelength of 295 nm, as a function of increasing concentration of the denaturant GdnHCl. As it can straightforwardly be seen the spectra display a red shift that is relevant of an increasing population of denatured protein molecules where tryptophan residues are exposed to the solvent. The statistically-weighted average wavelength $\langle\lambda\rangle=\sum F_i\lambda_i/\sum F_i$ where F_i is the fluorescence intensity has been used as the most adequate parameter to express the changes in the population of the denatured molecules as the concentration of GdnHCl was increased [41]. For each concentration C of GdnHCl, $\langle\lambda\rangle$ was calculated at various time intervals until equilibration. The data were fitted using a simple single-exponential form

$$\langle\lambda\rangle=\langle\lambda\rangle_{eq}-\left(\langle\lambda\rangle_{eq}-\langle\lambda\rangle_0\right)\cdot e^{-k_{app}\cdot t} \tag{5}$$

here $\langle\lambda\rangle_0$ and $\langle\lambda\rangle_{eq}$ are the wavelengths at initial and equilibration time and $k_{app}=k_d+k_r$ the sum of folding and refolding rates. The fitting results to Eq. (5) are shown in Table 3 and the fits themselves are illustrated in Fig. 6, top panel. Interestingly at the more dilute concentration regime, below 2 M, aggregation phenomena involving the chemically denatured molecules are also recorded at characteristic times that are longer than 150 h (data not shown). The reversibility of the chemical denaturation profile

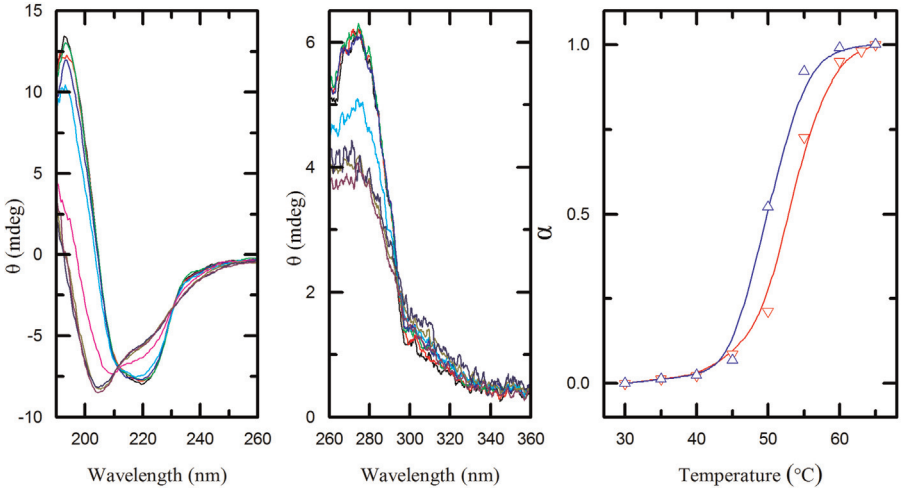

Fig. 5. Far-UV (left panel) and near-UV (middle panel) spectra for the TIM-barrel domain of *Mm*Chi60Cat in 20 mM sodium phosphate 1 mM EDTA pH 8.0 buffer at various temperatures above and below the thermal transition: 30 °C black, 35 °C red, 40 °C green, 45 °C blue, 50 °C cyan, 55 °C magenta, 60 °C dark yellow, 63 °C navy and 65 °C purple. Right panel: normalized ellipticity results at wavelengths 200 nm (down triangles) and 272 nm (up triangles) vs. temperature, demonstrating thermal hysteresis between conformational changes in the secondary and tertiary structures. Solid lines are guides to the eye. (For interpretation of the references to color in this figure legend, the reader is referred to the web version of this article.)

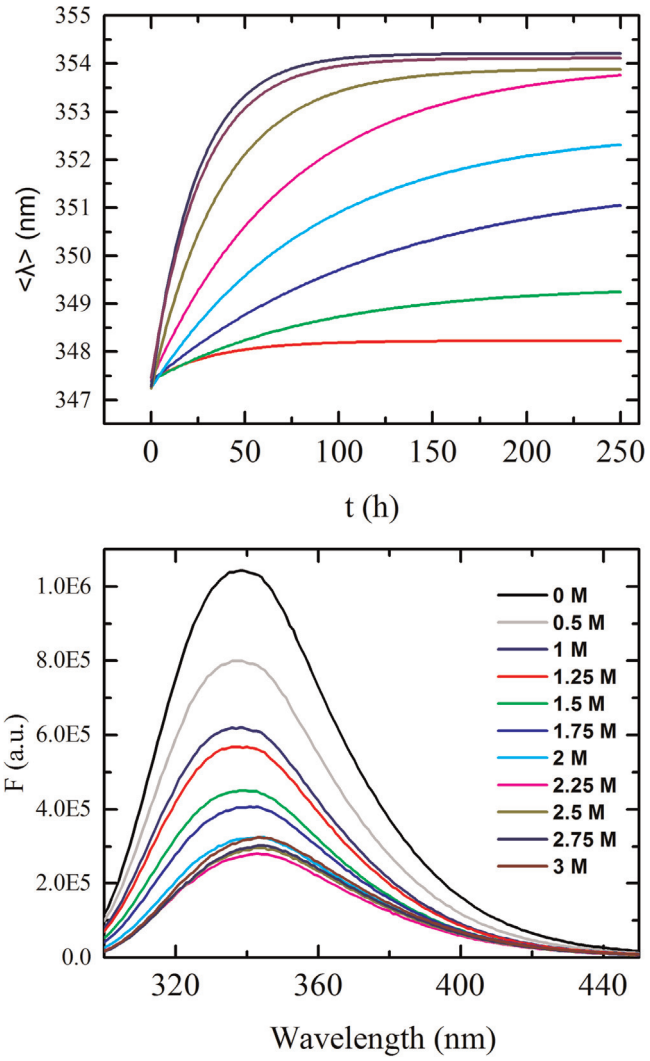

Fig. 6. Bottom panel: Chemical denaturation of the TIM-barrel domain of *Mm*Chi60 in 20 mM sodium phosphate 1 mM EDTA pH 8.0 buffer: Raw tryptophan-fluorescent spectroscopy data, emission spectra, equilibrated after considerably long times, normalized to the initial protein solution concentration of 0.08 mg/ml demonstrate a red wavelength shift as the concentration of GdnHCl is increased. Top panel: Single-exponential equilibration fits of the statistically-weighted average wavelength $\langle\lambda\rangle$ as a function of time, for the concentrations of GdnHCl added at time $t=0$ to the protein solution, during the chemical denaturation of the $(\beta/\alpha)_8$ barrel of *Mm*Chi60. The characteristic half-lives for the exponential equilibration are as long as four days, indicative of an extraordinarily high resistance to the chemical denaturant. (For interpretation of the references to color in this figure legend the reader is referred to the web version of theis article.)

Table 3
Equilibration values of $\langle\lambda\rangle_{eq}$ and the corresponding characteristic half-lives ($t_{1/2}$) at various GdnHCl concentrations.

C_{GdnHCl} (*M*)	λ_{eq} (*nm*)	$t_{1/2}$ (*h*)
0	347.5	–
0.5	348.0	–
1	348.0	–
1.25	348.3 ± 0.1	40.8
1.5	349.3 ± 0.4	57.8
1.75	351.6 ± 0.1	86.6
2	352.8 ± 0.3	69.3
2.25	353.6 ± 0.3	46.2
2.5	353.9 ± 0.2	27.7
2.75	354.2 ± 0.1	17.3
3	354.1 ± 0.2	18.7

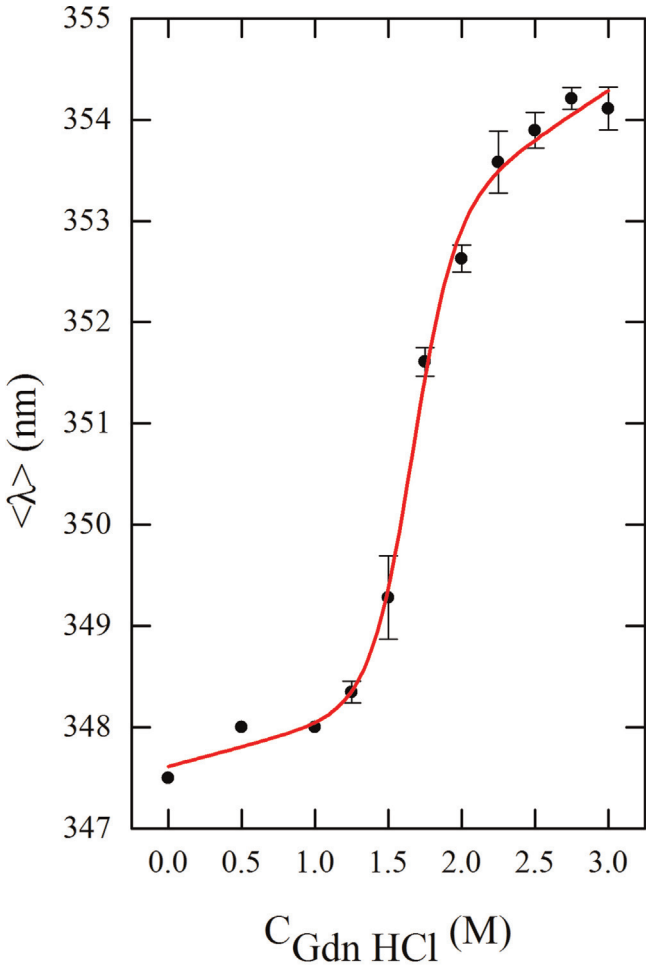

Fig. 7. Chemical denaturation of the TIM-barrel domain of *Mm*Chi60 in 20 mM sodium phosphate 1 mM EDTA pH 8.0 buffer. The isothermal sigmoidal plot, $\langle\lambda\rangle_{eq}$ vs. the concentration of GdnHCl and the corresponding non-linear-least squares fit to a two-state model yielding a measurement for the thermodynamic stability $\Delta G=6.75 \pm 1.3$ kcal/mol kcal/mol. (For interpretation of the references to color in this figure the reader is referred to the web version of this article.).

allows for the extraction of meaningful thermodynamic stability measurements. A two-state model has been used successfully to analyze the chemical unfolding data $\langle\lambda\rangle_{eq}$ vs. C_{GdnHCl} [42–44] presented in Fig. 7 yielding a value for the thermodynamic stability $\Delta G=6.75 \pm 1.3$ kcal/mol. The result from the non-linear least squares fit is also illustrated in Fig. 7 (solid red line). This value is lower from what was measured for the mesophilic Chi40 [23] and the hyperthermophilic HisF [22]. As in the case of HisF, the equilibrium unfolding of the TIM-barrel of *Mm*Chi60 conforms very well with two-state model [22]. This is significant of the fact that possible on-pathway intermediate states detected in the folding experiments of HisF are most likely sparsely populated in equilibrium unfolding. On the other hand, the kinetically driven thermal unfolding processes are prompt to reveal intermediate states. Notably the unfolding kinetics observed for *Mm*Chi60 are in line to analogous, extremely slowly processes encountered for thermostable proteins [22], [45–48]. These findings support the notion that protection mechanisms against thermal denaturation involve a high-kinetic barrier to unfolding. Apparently this is true for the psychrophilic TIM-barrels of *Mm*Chi60.

The *Mm*Chi60 E153Q is a low-activity mutant that has been successfully used to obtain the crystallographic structure of the full-length shallow binding groove of the $(\beta/\alpha)_8$ catalytic domain, unliganded as well as in complex with NAG_4 and NAG_5 [25]. The replacement of the carbonyl group by a neutral amide group

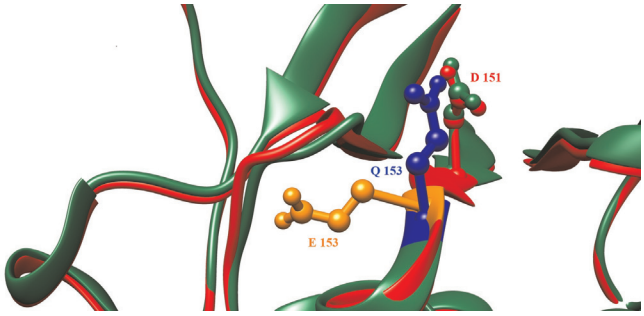

Fig. 8. Detail of the crystal structure of *Mm*Chi60 (PDB entry 4hmc) depicting the E153Q mutant superimposed on the wild type. The substitution of the charged glutamic acid by a glutamine flips the residue towards the Asp151 residue at the active center drastically reducing the enzymatic activity, (Ref. [25], PDB entry 4mb3).

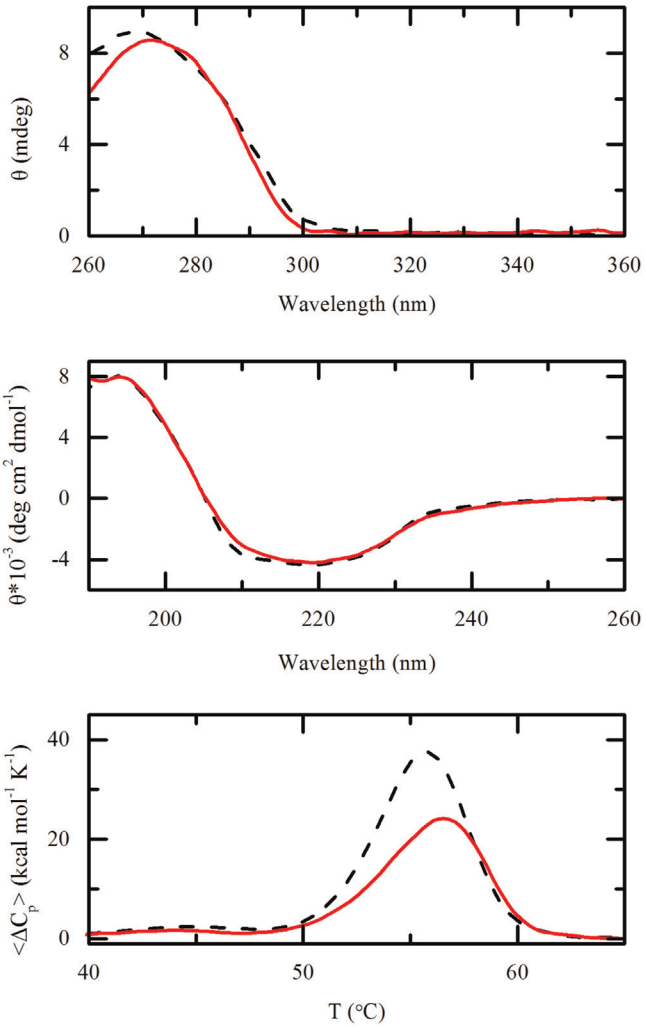

Fig. 9. Normalized far- (middle panel) and near-UV (top panel) CD spectra for the denaturation of the *Mm*Chi60_E153Q mutant (red solid line) in 20 mM sodium phosphate 1 mM EDTA pH 8.0 buffer (black dashed line) at room temperature. Bottom panel, DSC profiles comparing the thermal denaturation of the E153Q mutant and the wild type. It is evident that the mutated active site residue has a substantial impact upon the main calorimetric peak, which is associated to the unfolding of the TIM-barrel (For interpretation of the references to color in this figure legend, the reader is referred to the web version of this article.)

induces structural rearrangement at the active center by abolishing the flipping of the active-site residue upon ligand binding (Fig. 8). We have used CD and high-accuracy adiabatic DSC to explore the impact of this point mutation upon the overall structure as well as the stability of the molecule. The results are summarized in Fig. 9. It is evident from the far- and near-UV CD data that the mutant maintains the overall structure of the wild type. Minimal changes are recoded in the CD spectra at room temperatures. The reversible DSC profiles though (Fig. 9, bottom panel) paint a very different picture. While T_1 for the E153Q mutant remains relatively constant at 56.4 °C, as compared to the wild type and is also independent of the protein concentration indicating a monomeric state, the calorimetric enthalpy is reduced to 90.8 ± 8.8 kcal/mol, which is indicative of a substantial decrease in the thermodynamic stability of the molecule. Not surprisingly, the lower temperature peaks are preserved (data for the lowest-T peak not shown in Fig. 9) while the mutant's main peak is broader and more asymmetric than the wild type, evidence for a less cooperative thermal transition, likely affected by more severe kinetic processes.

The systematic thermodynamic studies of the psychrophilic *Mm*Chi60 and its mutants have led to interesting findings. Hinge structural regions not only provide for the mechanical flexibility of the molecule in solution but they also guarantee a thermodynamic "individuality" of the domains that they connect. Each of these domains, in the case of *Mm*Chi60, the CBM, the two Ig-like and the TIM-barrel appear to be able to unfold in a fully uncooperative fashion, not in the least affected by the thermal transitions of the others. The shallow-binding-groove β/α- barrel, bare of any of the $(\alpha+\beta)$ insertions encountered in other chitinases appears to have some extraordinary properties. While the thermodynamic stability is not particularly high, the structural motif is very highly resistant to chemical-induced denaturation. The thermal unfolding is characterized by a molten-globule-like stable intermediate state that may well assist in the understanding of the folding properties of the TIM-barrel, with important implications in protein-engineering applications.

Acknowledgments

F.S. and M.T. acknowledge support from the ARISTEIA I grant number 1692, administered by the General Secretariat of Research and Technology of Greece, co-financed by the European Social Fund and the State of Greece. The project was also funded in part by the European Union in the framework of the European Regional Development Fund.

Appendix A. Supplementary material

Supplementary data associated with this article can be found in the online version at http://dx.doi.org/10.1016/j.bbrep.2015.07.016.

References

[1] R.A.A. Muzzarelli, Chitin, Pergamon Press, Oxford, 1977.
[2] N.O. Keyhani, S. Roseman, Physiological aspects of chitin catabolism in marine bacteria, Biochim. Biophys. Acta 1473 (1999) 108–122.
[3] Y. Shigemasa, S. Minami, Applications of chitin and chitosan for biomaterials, Biotechnol. Genet. Eng. Rev. 13 (1996) 383–420.
[4] C. Gerday, M. Aittaleb, J.L. Arpigny, E. Baise, J.P. Chessa, G. Garsoux, I. Petrescu, G. Feller, Psychrophilic enzymes: a thermodynamic challenge, Biochim. Biophys. Acta 1342 (1997) 119–131.
[5] A. Bendt, H. Huller, U. Kammel, E. Helmke, T. Schweder, Cloning, expression, and characterization of a chitinase gene from the Antarctic psychrotolerant bacterium Vibrio sp. strain Fi:7, Extremophiles 5 (2001) 119–126.
[6] T. Lonhienne, K. Mavromatis, C.E. Vorgias, L. Buchon, C. Gerday, V. Bouriotis, Cloning, sequences, and characterization of two chitinase genes from the Antarctic Arthrobacter sp. strain TAD20: isolation and partial characterization of the enzymes, J. Bacteriol. 183 (2001) 1773–1779.
[7] H. Orikoshi, N. Baba, S. Nakayama, H. Kashu, K. Miyamoto, M. Yasuda,

Y. Inamori, H. Tsujibo, Molecular analysis of the gene encoding a novel cold-adapted chitinase (ChiB) from a marine bacterium, Alteromonas sp. strain O-7, J. Bacteriol. 185 (2003) 1153–1160.
[8] B. Henrissat, A. Bairoch, New families in the classification of glycosyl hydrolases based on amino acid sequence similarities, Biochem. J. 293 (1993) 781–788.
[9] B. Henrissat, G. Davies, Structural and sequence-based classification of glycoside hydrolases, Curr. Opin. Struct. Biol. 7 (1997) 637–644.
[10] G. Davies, B. Henrissat, Structures and mechanisms of glycosyl hydrolases, Structure 3 (1995) 853–859.
[11] A. Perrakis, I. Tews, Z. Dauter, A.B. Oppenheim, I. Chet, K.S. Wilson, C.E. Vorgias, Crystal structure of a bacterial chitinase at 2.3 A resolution, Structure 2 (1994) 1169–1180.
[12] A. Perrakis, C. Constantinides, A. Athanasiades, S.J. Hamodrakas, PBM: a software package to create, display and manipulate interactively models of small molecules and proteins on IBM-compatible PCs, Comput. Appl. Biosci. 11 (1995) 141–145.
[13] B.L. Cantarel, P.M. Coutinho, C. Rancurel, T. Bernard, V. Lombard, B. Henrissat, The Carbohydrate-Active EnZymes database (CAZy): an expert resource for Glycogenomics, Nucleic Acids Res. 37 (2009) D233–D238.
[14] K. Akagi, J. Watanabe, M. Hara, Y. Kezuka, E. Chikaishi, T. Yamaguchi, H. Akutsu, T. Nonaka, T. Watanabe, T. Ikegami, Identification of the substrate interaction region of the chitin-binding domain of Streptomyces griseus chitinase C, J. Biochem. 139 (2006) 483–493.
[15] P.H. Malecki, J.E. Raczynska, C.E. Vorgias, W. Rypniewski, Structure of a complete four-domain chitinase from Moritella marina, a marine psychrophilic bacterium, Acta Crystallogr. D 69 (2013) 821–829.
[16] T. Toratani, Y. Kezuka, T. Nonaka, Y. Hiragi, T. Watanabe, Structure of full-length bacterial chitinase containing two fibronectin type III domains revealed by small angle X-ray scattering, Biochem. Biophys. Res. Commun. 348 (2006) 814–818.
[17] R.K. Wierenga, The TIM-barrel fold: a versatile framework for efficient enzymes, FEBS Lett. 492 (2001) 193–198.
[18] R. Sterner, B. Hocker, Catalytic versatility, stability, and evolution of the (betaalpha)8-barrel enzyme fold, Chem. Rev. 105 (2005) 4038–4055.
[19] J.A. Zitzewitz, P.J. Gualfetti, I.A. Perkons, S.A. Wasta, C.R. Matthews, Identifying the structural boundaries of independent folding domains in the alpha subunit of tryptophan synthase, a beta/alpha barrel protein, Protein Sci. 8 (1999) 1200–1209.
[20] A. Godzik, J. Skolnick, A. Kolinski, Simulations of the folding pathway of triose phosphate isomerase-type alpha/beta barrel proteins, Proc. Natl. Acad. Sci. USA 89 (1992) 2629–2633.
[21] P.L. Wintrode, T. Rojsajjakul, R. Vadrevu, C.R. Matthews, D.L. Smith, An obligatory intermediate controls the folding of the alpha-subunit of tryptophan synthase, a TIM barrel protein, J. Mol. Biol. 347 (2005) 911–919.
[22] L. Carstensen, G. Zoldak, F.X. Schmid, R. Sterner, Folding mechanism of an extremely thermostable (betaalpha)(8)-barrel enzyme: a high kinetic barrier protects the protein from denaturation, Biochemistry 51 (2012) 3420–3432.
[23] S. Pyrpassopoulos, M. Vlassi, A. Tsortos, Y. Papanikolau, K. Petratos, C. E. Vorgias, G. Nounesis, Equilibrium heat-induced denaturation of chitinase 40 from Streptomyces thermoviolaceus, Proteins 64 (2006) 513–523.
[24] A.C. Zees, S. Pyrpassopoulos, C.E. Vorgias, Insights into the role of the (alpha+beta) insertion in the TIM-barrel catalytic domain, regarding the stability and the enzymatic activity of chitinase A from Serratia marcescens, Biochim. Biophys. Acta 1794 (2009) 23–31.
[25] P.H. Malecki, C.E. Vorgias, M.V. Petoukhov, D.I. Svergun, W. Rypniewski, Crystal structures of substrate-bound chitinase from the psychrophilic bacterium Moritella marina and its structure in solution, Acta Crystallogr. D 70 (2014) 676–684.
[26] E. Stefanidi, C.E. Vorgias, Molecular analysis of the gene encoding a new chitinase from the marine psychrophilic bacterium Moritella marina and biochemical characterization of the recombinant enzyme, Extremophiles 12 (2008) 541–552.
[27] H.E. Klock, S.A. Lesley, The Polymerase Incomplete Primer Extension (PIPE) method applied to high-throughput cloning and site-directed mutagenesis, Methods Mol. Biol. 498 (2009) 91–103.
[28] K. Poole, R.E. Hancock, Phosphate transport in Pseudomonas aeruginosa. Involvement of a periplasmic phosphate-binding protein, Eur. J. Biochem. 144 (1984) 607–612.
[29] C.H.E. Gasteiger, A. Gattiker, S. Duvaud, M.R. Wilkins, R.D. Appel, A. Bairoch, Protein identification and analysis tools on the ExPASy server, in the proteomics protocols handbook, in: J.M. Walker (Ed.), Humana Press, 2007, pp. 571–607.
[30] K. Takahashi, J.M. Sturtevant, Thermal denaturation of streptomyces subtilisin inhibitor, subtilisin BPN', and the inhibitor-subtilisin complex, Biochemistry 20 (1981) 6185–6190.
[31] A.D. Robertson, K.P. Murphy, Protein structure and the energetics of protein stability, Chem. Rev. 97 (1997) 1251–1268.
[32] J.C. Bischof, X. He, Thermal stability of proteins, Ann. New York Acad. Sci. 1066 (2005) 12–33.
[33] X. He, J.C. Bischof, Quantification of temperature and injury response in thermal therapy and cryosurgery, Crit. Rev. Biomed. Eng. 31 (2003) 355–422.
[34] V.Y. Grinberg, T.V. Burova, T. Haertle, V.B. Tolstoguzov, Interpretation of DSC data on protein denaturation complicated by kinetic and irreversible effects, J. Biotechnol. 79 (2000) 269–280.
[35] J.K. Kaushik, K. Ogasahara, K. Yutani, The unusually slow relaxation kinetics of the folding-unfolding of pyrrolidone carboxyl peptidase from a hyperthermophile, *Pyrococcus furiosus*, J. Mol. Biol. 316 (2002) 991–1003.
[36] P.L. Privalov, S.A. Potekhin, Scanning microcalorimetry in studying temperature-induced changes in proteins, Methods Enzymol. 131 (1986) 4–51.
[37] N. Sreerama, R.W. Woody, Computation and analysis of protein circular dichroism spectra, Methods Enzymol. 383 (2004) 318–351.
[38] A.V. Finkelstein, O.B. Ptitsyn, Protein physics, Academic Press, London (2002), p. 207–225.
[39] M. Arai, K. Kuwajima, Role of the molten globule state in protein folding, Adv. Protein Chem. 53 (2000) 209–282.
[40] E. Freire, A. Schon, B.M. Hutchins, R.K. Brown, Chemical denaturation as a tool in the formulation optimization of biologics, Drug Discov. Today 18 (2013) 1007–1013.
[41] C.A. Royer, C.J. Mann, C.R. Matthews, Resolution of the fluorescence equilibrium unfolding profile of trp aporepressor using single tryptophan mutants, Protein Sci. 2 (1993) 1844–1852.
[42] J. Clarke, A.R. Fersht, Engineered disulfide bonds as probes of the folding pathway of barnase: increasing the stability of proteins against the rate of denaturation, Biochemistry 32 (1993) 4322–4329.
[43] A. Fersht, Structure and Mechanism in Protein Science, W. H. Freeman and Comapny, New York (1999) pp 508–517.
[44] A. Thanassoulas, M. Nomikos, M. Theodoridou, D. Yannoukakos, D. Mastellos, G. Nounesis, Thermodynamic study of the BRCT domain of BARD1 and its interaction with the -pSER-X-X-Phe- motif-containing BRIP1 peptide, Biochim. Biophys. Acta 1804 (2010) 1908–1916.
[45] A. Mukaiyama, K. Takano, M. Haruki, M. Morikawa, S. Kanaya, Kinetically robust monomeric protein from a hyperthermophile, Biochemistry 43 (2004) 13859–13866.
[46] D. Perl, C. Welker, T. Schindler, K. Schroder, M.A. Marahiel, R. Jaenicke, F. X. Schmid, Conservation of rapid two-state folding in mesophilic, thermophilic and hyperthermophilic cold shock proteins, Nat. Struct. Biol. 5 (1998) 229–235.
[47] T. Dams, R. Jaenicke, Stability and folding of dihydrofolate reductase from the hyperthermophilic bacterium Thermotoga maritima, Biochemistry 38 (1999) 9169–9178.
[48] W.A. Deutschman, F.W. Dahlquist, Thermodynamic basis for the increased thermostability of CheY from the hyperthermophile Thermotoga maritima, Biochemistry 40 (2001) 13107–13113.